EPJ manuscript No.
(will be inserted by the editor)

Target Fragmentation in pp, ep and γp Collisions at High Energies

U. D'Alesio and H.J. Pirner

Institut für Theoretische Physik, Universität Heidelberg, Philosophenweg 19, 69120 Heidelberg, Germany

Received: date / Revised version: date

Abstract. We calculate target fragmentation in $pp \to nX$ and $\gamma p \to nX$ reactions in the meson cloud picture of the nucleon. The $pp \to nX$ reaction is used to fix the $pn\pi^+$ form factor for three different models. We take into account the possible destruction of the residual neutron by the projectile. Using the form factor from the hadronic reaction we calculate photoproduction and small $x_{\rm Bj}$ electroproduction of forward neutrons at HERA. Here the $q\bar{q}$ dipoles in the photon can rescatter on the residual neutron. In photoproduction we observe slightly less absorption than in the hadronic reaction. For deep inelastic events ($Q^2 > 10$ GeV^2) screening is weaker but still present at large Q^2. The signature for this absorptive rescattering is a shift of the $d\sigma/dE_n$ distribution to higher neutron energies for photofragmentation.

PACS. 13.60.Hb Total and inclusive cross sections – 11.80.La Multiple scattering

1 Introduction

In the last two decades the study of total inclusive deep inelastic scattering (DIS) processes has allowed to extract important information on the structure of hadrons. Parton distributions have been determined and scaling violations have been tested to a high level of accuracy. The QCD improved parton model has been shown to be very reliable in the presence of a hard scale.

On the other hand semi-inclusive reactions with electromagnetic probes are still less explored. They can improve our knowledge on the inner hadronic structure.
Through the study of new observables characterizing these processes we may ask more detailed questions about the proton. In this case the application of perturbative QCD (pQCD) has been restricted to high p_t events, and experiments have been analyzed in terms of parton distributions and fragmentation functions.

With the HERA collider target fragmentation can be studied in a much cleaner way than with fixed target experiments. New interest has been triggered by measurements on leading neutron production performed by the ZEUS and H1 collaborations at the electron-proton collider [1,2]. These data are currently analyzed in terms of hadronic degrees of freedom, i.e. studying the virtual pion flux in the nucleon [3,4]. Thus one hopes to extract information about the pion structure function at very small x, not reachable in Drell-Yan experiments.

Send offprint requests to: H.J. Pirner, Institut für Theoretische Physik, Universität Heidelberg, Philosophenweg 19, D-69120 Heidelberg
Correspondence to: umberto.dalesio@ca.infn.it

In the late fifties Chew and Low already suggested the idea of using pions from the pion cloud of the proton as targets to get information on the interaction of different projectiles with pions [5].
Novel theoretical tools to include forward leading particle production in the framework of standard pQCD have been developed by Trentadue, Veneziano and Graudenz [6, 7], who introduced a new set of nonperturbative distributions (fracture functions) which allow to absorb collinear singularities at leading order in the QCD coupling constant.

If we look at $\gamma^* p$ reactions in the cm-system, we can consider the incoming photon as a $q\bar{q}$ state [8] that interacts with a proton made up of two color neutral components, one of which is the final state neutron. This involves quite different aspects of the nucleon than those investigated in deep inelastic inclusive scattering. Especially long range properties of the baryon can be analyzed in such a process. At which length does the string connecting a quark to the residual diquark break and produce two colour neutral objects, a meson and a nucleon? This question is especially important for nuclear physics, as one wants to know what amount of the nucleon-nucleon interaction is describable in terms of meson exchange forces in the nucleus.

From the high-energy point of view the determination of the pion structure function is central. The common interpretation of the $\gamma^* p \to nX$ experiment relies on the application of the meson cloud model of the nucleon [9,10, 11] together with the factorization hypothesis that allows to separate the reaction into two steps: the fragmentation process and the interaction [12,13]. It assumes that the fragmentation process is universal, i.e. independent of the

projectile which initiates fragmentation. In the following we will examine the validity of this factorization hypothesis carefully.

Let us consider the generic reaction with an incoming projectile a leading to neutron production i.e. $ap \to nX$ (see fig. 1). In the one-pion-exchange model the differential cross section is given by the product of the pion flux factor times the total $a\pi$ cross section:

$$\frac{d\sigma^{ap\to nX}}{dz dp_t^2} = F_{n\pi}(z,p_t)\,\sigma_{\rm tot}^{a\pi}(s')\,. \qquad (1)$$

The flux factor $F_{n\pi}(z,p_t)$ gives the probability for the splitting of a proton into a pion-neutron system. It depends on the longitudinal momentum fraction z carried by the detected neutron and its transverse momentum[1] p_t. The total cross section $\sigma_{\rm tot}^{a\pi}(s')$ is a function of s' the center of mass sub-energy squared in the $a\,\pi^+$ interaction.

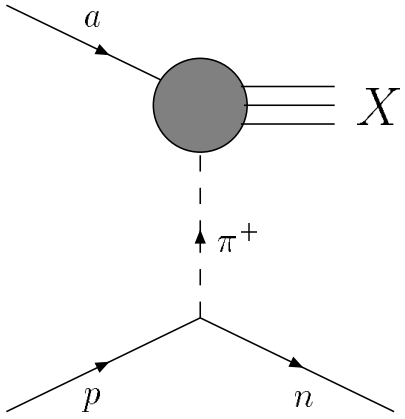

Fig. 1. Picture of semi-inclusive neutron production according to the one-pion-exchange model.

The usual procedure [3,4] is to fix the parameters entering the flux factor from the data of leading neutron production in proton-proton ($a = p$) collisions. Then assuming universality, one applies the same equation (1) to virtual photon scattering ($a = \gamma^*$) in DIS. Measuring the differential cross section $\gamma^* p \to nX$ one extracts the pion structure function, since $\sigma_{\rm tot}^{\gamma^*\pi^+}$ is proportional to $F_2^{\pi^+}$. Obviously the factorization hypothesis plays a crucial role in this method.

Indeed early works [14,15,16] on absorption effects for pion-exchange mechanism in hadronic inclusive reactions indicate a suppression factor of the order of 50-70%. Recently a first and detailed study of absorptive corrections in the Regge formalism [17] has appeared. Many of our conclusions agree with the ones reached in ref. [17]. These absorptive effects depend on the projectile and are a source of factorization breaking. They can be comparable or even more important than other background contributions, already estimated, reducing the accuracy of $F_2^{\pi^+}$ measurements. We will investigate the relevance of absorptive corrections in detail in order to understand the one-pion-exchange mechanism and the extraction of the pion structure function. We apply high-energy Glauber theory to calculate and compare the screening corrections in leading neutron production for $p\,p$ and $\gamma^{(*)}\,p$ reactions. We especially search for differences between photoproduction and deep inelastic scattering in neutron fragmentation. To this end we follow the Q^2-evolution of the fracture functions from a kinematic region where the perturbative evolution of [6,7] is not yet applicable to large Q^2. We find similarly to ref. [17] that absorptive corrections for highly virtual photons do not vanish, as indicated by data [1,18]. However this effect is smaller than what has been found for proton-proton interactions. This dependence on the projectile can be a source of factorization breaking. With respect to ref. [17], we extend this analysis to real photons ($Q^2 = 0$) and we find that the size of rescattering corrections is comparable to that of hadronic reactions and bigger than that of virtual photons.

The outline of the paper is as follows. In section 2 we describe the meson cloud model, in section 3 we calculate the absorptive corrections to $pp \to nX$. Section 4 is devoted to virtual and real photoproduction of forward neutrons. Section 5 closes with a summary and a discussion.

2 Meson Cloud Model

In this section we review briefly the main features of the meson cloud model (MCM).
In the MCM a proton is viewed as a bare proton surrounded by a virtual meson cloud,

$$\begin{aligned}|p\uparrow\rangle &= \sqrt{S}\Big\{|p_0\uparrow\rangle \\ &\quad + \sum_{\lambda\lambda'}\sum_{BM}\int dz d^2\mathbf{p}_t\,\phi_{BM}^{\lambda\lambda'}(z,\mathbf{p}_t)|B,M;z,\mathbf{p}_t\rangle\Big\} \\ &= \sqrt{S}\Big\{|p_0\uparrow\rangle + \sum_{\lambda\lambda'}\int dz d^2\mathbf{p}_t\,\phi_{N\pi}^{\lambda\lambda'}(z,\mathbf{p}_t) \\ &\quad \times\Big[\sqrt{\frac{1}{3}}|p,\pi^0;z,\mathbf{p}_t\rangle + \sqrt{\frac{2}{3}}|n,\pi^+;z,\mathbf{p}_t\rangle\Big] + \cdots\Big\}\,, \end{aligned} \qquad (2)$$

where $\phi_{BM}^{\lambda\lambda'}(z,\mathbf{p}_t)$ is the probability amplitude to find, inside a proton with spin up, a baryon B with longitudinal momentum fraction z, transverse momentum $\mathbf{p}_t$ and helicity λ and a meson M, with longitudinal momentum fraction $1-z$, transverse momentum $-\mathbf{p}_t$ and helicity λ'. We restrict ourselves to the first contributions of this expansion in terms of Fock states. $\sqrt{S}$ is the renormalization constant, which is fixed by $\langle p|p\rangle = 1$ and gives the amplitude for the bare proton.

In the light-cone approach the amplitudes $\phi_{N\pi}$, for a proton with spin $+1/2$, read [10]

$$\phi_{N\pi}^{1/2,0}(z,\mathbf{p}_t) = \frac{\sqrt{3}g_0}{4\pi\sqrt{\pi}}\frac{1}{\sqrt{z^2(1-z)}}\frac{m_N(z-1)}{M_{N\pi}^2 - m_N^2}$$

[1] We use $p_t = |\mathbf{p}_t|$.

$$\phi^{-1/2,0}_{N\pi}(z,\mathbf{p}_t) = \frac{\sqrt{3}g_0}{4\pi\sqrt{\pi}} \frac{1}{\sqrt{z^2(1-z)}} \frac{|\mathbf{p}_t| e^{-i\varphi}}{M^2_{N\pi} - m^2_N}\,, \quad (3)$$

where $M^2_{N\pi}$ is the invariant mass of the pion-nucleon system, given by

$$M^2_{N\pi} = \frac{m^2_N + p^2_t}{z} + \frac{m^2_\pi + p^2_t}{1-z}\,,$$

m_N and m_π are the nucleon and the pion masses; g_0 is the bare pion-nucleon coupling constant and φ is the azimuthal angle in the transverse plane. Including the renormalization factor $\sqrt{S}$ from eq. (2) we get the renormalized effective coupling $g = \sqrt{S} g_0$ [11], which can be extracted from low-energy data: we use $g^2/4\pi = 13.75$.

Because of the extended nature of the hadrons involved, the interaction amplitudes in eq. (3) have to be modified by including a phenomenological πNN form factor. It is important to stress here that while the vertex is derived from an effective meson-nucleon Lagrangian, the form factor is introduced *ad hoc*. In order to parametrize the form factor we need to introduce the momentum transfer t which can be expressed as follows

$$\begin{aligned} t = (p_N - p'_N)^2 &= -\frac{1}{z}\left[p^2_t + (1-z)^2 m^2_N\right] \\ &= (1-z)(m^2_N - M^2_{N\pi}) + m^2_\pi\,. \end{aligned}$$

Different models and parametrizations are available in the literature. In the following we compare the results obtained using the light-cone approach and the covariant approach, the last one with inclusion of reggeization. Besides these two form factors we consider a πNN form factor extracted from Skyrme-type models [19,20]. This form factor leaves low momentum transfers essentially unaffected while suppressing the high momentum region strongly. The three models are:

– light-cone πNN form factor

$$\begin{aligned} G(z,p_t) &= \exp[R^2_{lc}(m^2_N - M^2_{N\pi})] \\ &= \exp[R^2_{lc}(t - m^2_\pi)/(1-z)] \end{aligned} \quad (4)$$

– covariant πNN form factor

$$G(z,p_t) = \exp[R^2_c(t - m^2_\pi)] \quad (5)$$

– Skyrme model πNN form factor

$$G(z,p_t) = \exp[R^2_S\, t] g(t) \quad (6)$$

where $g(t)$ is a rational function of t given in the appendix.

The amplitudes $\phi^{\lambda\lambda'}$ must be changed according to $\phi^{\lambda\lambda'} \to \phi^{\lambda\lambda'}\, G(z,p_t)$. The flux in eq. (1), for proton fragmentation into a neutron can then be calculated as

$$F_{n\pi}(z,p_t) = \frac{2}{3}\pi \sum_{\lambda\lambda'} |\phi^{\lambda\lambda'}_{N\pi}(z,\mathbf{p}_t)|^2 |G(z,p_t)|^2\,, \quad (7)$$

where 2/3 is the isospin factor and the azimuthal angle in the transverse plane has been integrated out. The reggeization of the pion (relevant for $z \to 1$) is included in the covariant and Skyrme approaches by the further change

$$\phi^{\lambda\lambda'} \to \phi^{\lambda\lambda'}(1-z)^{-\alpha_\pi(t)}\,,$$

where $\alpha_\pi(t) = \alpha_\pi(0) + \alpha'_\pi t$ is the pion Regge-trajectory, with $\alpha_\pi(0) = 0$ and $\alpha'_\pi \simeq 1\,\mathrm{GeV}^{-2}$. The light-cone form factor contains the decrease of the cross section for $z \to 1$ already in the exponential. Its form, however, is a crude approximation and therefore we do not expect the light-cone form factor to be adequate for extremely large z.

In the following section we consider pp collisions in order to fix the parameters R_{lc} and R_c appearing in the previous equations[2].

3 Estimate of absorptive corrections in $pp \to nX$

We consider target fragmentation reactions as stripping reactions in the cm-system where the projectile proton strips a π^+ from the target proton leaving behind a neutron. The projectile proton smashes the pion into pieces, while the neutron remains intact as a spectator. Any additional interactions like $\Delta-$production or ρ-exchange may spoil this simple picture and reduce the accuracy of the determination of the πpn vertex. This has been studied and the amount of such a background is estimated to be around 20% [3,4]. We will neglect these processes in our calculation, but we model them rescaling the one-pion-exchange cross section by 1.2.

We are fully aware that this rescaling procedure is a poor simplification of the background contributions. A recent work [21] shows that an improved treatment of the background is important to get the right neutron distribution at very high z values. Nevertheless we will concentrate mainly on the region of $p_t = 0$ and $0.7 < z < 0.9$, where our simple rescaling gives reasonable results.

The invariant differential cross section for the one-pion-exchange mechanism is (in light-cone approach[3])

$$\begin{aligned} E_n \frac{d^3\sigma}{d^3\mathbf{p}_n} &= \frac{z}{\pi}\frac{d\sigma}{dz dp^2_t} \\ &= \frac{2g^2}{16\pi^2}\frac{1}{z(1-z)}\frac{m^2_N(1-z)^2 + p^2_t}{(M^2_{N\pi} - m^2_N)^2} |G(z,p_t)|^2 \sigma^{p\pi}_{\mathrm{tot}}\,. \end{aligned} \quad (8)$$

This picture is reliable when the pion and the neutron in the *target* proton are well separated, i.e. at large z and large impact parameter. For small impact parameters and intermediate z values it must be extended to allow the scattering of the projectile on the neutron and the consequent screening effect (see fig. 2).

To be more precise we distinguish in our notation between the target ($p_{(T)}$) and projectile ($p_{(P)}$) proton:

$$p_{(P)}\, p_{(T)} \to nX\,.$$

[2] For the Skyrme form factor we use the value fitted in [19]: $R^2_s = 0.031/m^2_\pi$.

[3] Reggeized covariant expression can be obtained multiplying eq. (8) by $(1-z)^{-2\alpha_\pi(t)}$ and taking $G(z,p_t)$ from eq. (5).

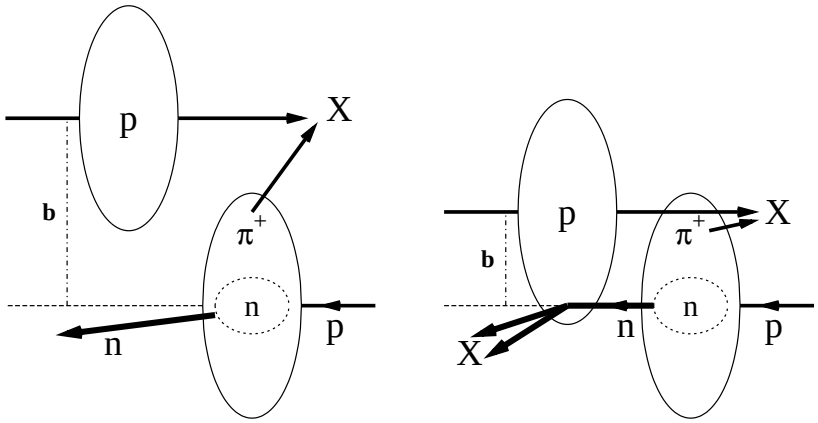

Fig. 2. Picture of the collision for two different impact parameters. On the left we show a peripheral collision (large **b**) where the pion is stripped and the neutron acts as a spectator. On the right we show a more central collision where the projectile proton can destroy the neutron through rescattering.

We employ the high-energy Glauber approximation to multiple scattering which has been used for target fragmentation in heavy ion collisions in ref. [22].

A more formal derivation of absorptive corrections can be found in [17], where Regge calculus and generalized AGK cutting rules [23] are applied. Our approach can be traced back to that of [17] and viewed as a simplification of it in the eikonal approximation.

We treat the target proton as a pion-neutron system (ϕ_0) undergoing a transition to an excited state (ϕ_α). The cross section for this process can be expressed as

$$\begin{aligned}\sigma(\phi_0 \to \phi_\alpha) &= \int d^2\mathbf{b}\, \sigma_{0\to\alpha}(\mathbf{b}) \\ &= \int d^2\mathbf{b}\, \left|\langle\phi_\alpha[1 - S^{p\pi}S^{pn}]|\phi_0\rangle\right|^2 , \end{aligned} \quad (9)$$

where $\mathbf{b}$ is the impact parameter and S^{ab} are the interaction operators (see below). We assume that the proton state ϕ_0 can be factorized into a system of a pion and a neutron

$$|\phi_0\rangle \equiv |\psi_0^{\rm sp}\pi_0 n_0\rangle = |\psi_0^{\rm sp}\rangle|\pi_0\rangle|n_0\rangle\,,$$

with $\psi_0^{\rm sp}$ the spatial component, specified to keep spatial and intrinsic degrees of freedom separated. Similarly the excited state with an undisturbated neutron has the form:

$$|\phi_\alpha\rangle \equiv |\psi_j^{\rm sp}\pi_{\alpha'} n_0\rangle = |\psi_j^{\rm sp}\rangle|\pi_{\alpha'}\rangle|n_0\rangle\,,$$

where we have introduced an extra index (j) to take into account all possible spatial configurations for this excited state; $|\pi_{\alpha'}\rangle$ is an arbitrary state with the same quantum numbers as the pion. To get the total cross section we sum now over all spatial configurations and over all $|\pi_{\alpha'}\rangle$ states. We apply the closure relation and exclude the elastic contribution ($|\pi_0\rangle$)

$$\begin{aligned}\sigma(\mathbf{b}) = \sum_\alpha \sigma_{0\to\alpha}(\mathbf{b}) &= \sum_{\alpha'\neq 0}\sum_j \Big|\int d^3y_n d^3y_\pi \\ &\quad \psi_j^*(y_n,y_\pi)\psi_0(y_n,y_\pi) S^{p\pi}_{\alpha' 0}(\mathbf{b}-\mathbf{s}_\pi) S^{pn}_{00}(\mathbf{b}-\mathbf{s}_n)\Big|^2 \\ &= \sum_{\alpha'\neq 0}\int d^3y_n d^3y_\pi |\psi_0(y_n,y_\pi)|^2 \\ &\quad \times S^{p\pi}_{\alpha' 0}(\mathbf{b}-\mathbf{s}_\pi) S^{\dagger p\pi}_{0\alpha'}(\mathbf{b}-\mathbf{s}_\pi) |S^{pn}_{00}(\mathbf{b}-\mathbf{s}_n)|^2 \\ &= \int d^3y_n d^3y_\pi |\psi_0(y_n,y_\pi)|^2 \\ &\quad \times \left[1 - |S^{p\pi}_{00}(\mathbf{b}-\mathbf{s}_\pi)|^2\right] |S^{pn}_{00}(\mathbf{b}-\mathbf{s}_n)|^2 , \end{aligned} \quad (10)$$

where $y_n \equiv (\mathbf{s}_n, z_n)$, $y_\pi \equiv (\mathbf{s}_\pi, z_\pi)$, $\mathbf{s}_\pi$ and $\mathbf{s}_n$ are the coordinates of the pion and the neutron in the impact parameter plane; z_n and z_π are their longitudinal momentum fractions. Also

$$\begin{aligned} 1 - |S^{p\pi}_{00}|^2 &= 1 - |1 - \Gamma^{p\pi}|^2 \simeq 2Re\Gamma^{p\pi} \\ |S^{pn}_{00}|^2 &= |1 - \Gamma^{pn}|^2 \simeq 1 - 2Re\Gamma^{pn}\,, \end{aligned} \quad (11)$$

where the profile functions Γ describe the respective two-body scatterings and are related to the scattering amplitudes in momentum space by Fourier transformation

$$f^{ij}(\mathbf{q}) = \frac{ip_{\rm cm}}{2\pi}\int d^2\mathbf{b}\, e^{i\mathbf{q}\cdot\mathbf{b}}\, \Gamma^{ij}(\mathbf{b})\,. \quad (12)$$

Let us now consider the density distribution $|\psi_0(y_n,y_\pi)|^2$. We parametrize this density starting from the probability density to find a pion and a neutron at a certain transverse separation $\mathbf{b}_{rel} = \mathbf{s}_n - \mathbf{s}_\pi$, imposing the center-of-mass constraint in $\mathbf{b}$-space and the longitudinal momentum conservation: $\mathbf{b}_{cm} = z_n\mathbf{s}_n + z_\pi\mathbf{s}_\pi = 0$, $z_n + z_\pi = 1$,

$$|\psi_0(y_n,y_\pi)|^2 \equiv \rho_{n\pi}(z_n,\mathbf{b}_{rel})\delta^2(z_n\mathbf{s}_n + z_\pi\mathbf{s}_\pi)\delta(z_n + z_\pi - 1)\,. \quad (13)$$

Inserting eqs. (11) and (13) into eq. (10) and carrying out the 3-dimensional integration over y_π, we get for the semi-inclusive cross section

$$\frac{d\sigma^{pp\to nX}}{dz} = \int d^2\mathbf{b}\, \frac{d\sigma(\mathbf{b})}{dz}\,, \qquad \text{with} \quad (14)$$

$$\frac{d\sigma(\mathbf{b})}{dz} = \int d^2\mathbf{s}_n \frac{1}{(1-z)^2}\,\rho_{n\pi}(z,\mathbf{b}_{rel}) \times 2Re\Gamma^{p\pi}(\mathbf{b}-\mathbf{s}_\pi)\,[1-2Re\Gamma^{pn}(\mathbf{b}-\mathbf{s}_n)] = \int d^2\mathbf{b}_{rel}\rho_{n\pi}(z,\mathbf{b}_{rel})\,2Re\Gamma^{p\pi}(\mathbf{b}+z\mathbf{b}_{rel}) \times [1-2Re\Gamma^{pn}(\mathbf{b}-(1-z)\mathbf{b}_{rel})]\,, \quad (15)$$

where we have restored the previous notation, $z_n \equiv z$ and replaced the pion and neutron coordinates by

$$\mathbf{b}_{rel} = -\frac{\mathbf{s}_\pi}{z} = \frac{\mathbf{s}_n}{1-z}\,.$$

3.1 Pion-neutron density and profile functions in b-space

In order to extract quantitative information from eq. (15) we evaluate the probability density to find a pion and neutron at a certain distance inside the parent proton. The main idea is to start with the amplitudes in momentum space for the splitting of a proton into a pion-neutron system (see eqs. (3)) and then calculate the Fourier transform in two dimensions with respect to the transverse momentum.
We obtain the amplitudes in $\mathbf{b}$-space (we keep z fixed)

$$\psi^i_{n\pi}(z,\mathbf{b}_{rel}) = \frac{1}{2\pi}\int d^2\mathbf{p}_t e^{i\mathbf{b}_{rel}\cdot\mathbf{p}_t}\phi^i_{n\pi}(z,\mathbf{p}_t)\,,$$

where by $\phi^i_{n\pi}$ we mean $\sqrt{2/3}\phi^{\lambda\lambda'}_{N\pi}$. From this we obtain the probability density to find a neutron and a pion respectively with longitudinal momentum z and $1-z$ and relative transverse separation $\mathbf{b}_{rel}$:

$$\rho_{n\pi}(z,\mathbf{b}_{rel}) = \sum_i |\psi^i_{n\pi}(z,\mathbf{b}_{rel})|^2\,.$$

In fig. 3 we show the behaviour of these densities at different values of z for the light-cone and the covariant approach.

Concerning the profile functions we start from scattering amplitudes with gaussian shapes,

$$f^{ab}(\mathbf{q}) = \frac{ip_{\rm cm}}{4\pi}\sigma^{ab}_{\rm tot}\exp\left[-\frac{\mathbf{q}^2}{2\Lambda^2_{ab}}\right] \quad (16)$$

and by Fourier transformation we get

$$\Gamma^{ab}(\mathbf{b}) = \frac{1}{4\pi}\sigma^{ab}_{\rm tot}\Lambda^2_{ab}\exp\left[-\frac{\mathbf{b}^2\Lambda^2_{ab}}{2}\right]\,, \quad (17)$$

where we have considered purely imaginary amplitudes as we are interested in the high-energy regime.

3.2 Cross section for $pp \to nX$

The gaussian dependence of the profile functions allows us to perform the $\mathbf{b}$-integration in eq. (14) analytically, we have then

$$\frac{d\sigma^{pp\to nX}}{dz} = \int d^2\mathbf{b}_{rel}\rho_{n\pi}(z,\mathbf{b}_{rel})\,\sigma^{p\pi^+}_{\rm tot} \times \Big\{1-\Lambda^2_{\rm eff}\frac{\sigma^{pn}_{\rm tot}}{2\pi}\exp\Big[-\frac{\Lambda^2_{\rm eff}\mathbf{b}^2_{rel}}{2}\Big]\Big\}\,, \quad (18)$$

with

$$\Lambda^2_{\rm eff} = \frac{\Lambda^2_{p\pi}\Lambda^2_{pn}}{\Lambda^2_{p\pi}+\Lambda^2_{pn}} \qquad [\Lambda^2_{p\pi}\approx\Lambda^2_{pn}\approx 0.08\,{\rm GeV}^2]\,. \quad (19)$$

Before giving explicit results from eq. (18), let us try to interprete the physical picture emerging from it.
The first term alone is nothing else than the standard expression according to the factorization hypothesis, eq. (1), i.e. the stripping of the pion cloud inside the target proton. The second term represents the screening correction which is the most interesting result of our calculation. The Born fragmentation cross section is multiplied by the probability that the projectile proton does not destroy the neutron component of the target proton. The screening factor changes the simple factorization picture.

Assuming that the final state interaction does not modify the transverse momentum distribution of the fragments, we can calculate the invariant differential cross section $E_n\frac{d^3\sigma}{d^3\mathbf{p}_n}$ by multiplying the differential cross sections for the longitudinal distributions with the transverse probability distribution for the fragmentation process. This method seems to work quite well in nuclear target fragmentation [22]. We get

$$E_n\frac{d^3\sigma^{pp\to nX}}{d^3\mathbf{p}_n} = \frac{z}{\pi}\frac{1}{N(z)}\frac{dN(z,p_t)}{dp_t^2}\,\frac{d\sigma^{pp\to nX}}{dz}\,, \quad (20)$$

where $d\sigma/dz$ is given by eq. (18). The normalized fraction of fragmentation processes in the interval p_t, p_t+dp_t is obtained from the normalized pion flux factor:

$$\frac{1}{N(z)}\frac{dN(z,p_t)}{dp_t^2} = \frac{F_{n\pi}(z,p_t)}{\int dp_t^2 F_{n\pi}(z,p_t)}\,. \quad (21)$$

Definitely the experimental cross sections for $p_t = 0$ [24,25] have the most pronounced shape. Here one can really see a fragmentation peak which seems to be superimposed on some background. We estimate additional contributions[4] to have a similar shape as the calculated cross section and lead to a 20% correction. Thus we scale our result for the one-pion-exchange contribution by a factor 1.2. A model calculation of background processes can be found in ref. [21]. For larger p_t values the fragmentation cross sections become rapidly flatter and smaller and the background increases. Therefore we fit the radius parameters to the $p_t = 0$ data. In fig. 4 we show the semi-inclusive cross section for $pp \to nX$ as a function of the longitudinal momentum fraction z of the neutron together with the experimental data from ref. [24]. For the

[4] These may come from resonance excitations like $p \to \pi^+\Delta^0$ and $p \to \pi^+ N^{*0}$, which decay into neutrons.

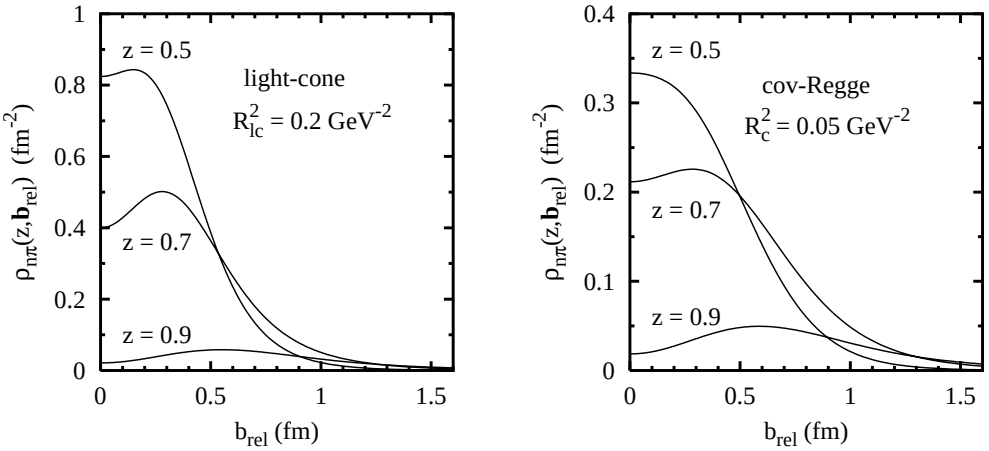

Fig. 3. Pion-neutron densities in the transverse plane for various z values in light-cone (left) and covariant approach (right).

total cross sections $\sigma^{p\pi^+}_{\rm tot}$ and $\sigma^{pn}_{\rm tot}$ we adopt the fits[5] performed in ref. [27]. We adjust the radius parameters R_{lc} in the light-cone and R_c in the covariant form factor to the data and find a reasonable agreement with the following values: $R^2_{lc} = 0.2\,\mathrm{GeV}^{-2}$ and $R^2_c = 0.05\,\mathrm{GeV}^{-2}$. An important feature of the screening correction is that its inclusion reduces the radius parameters so extracted. The shape of the Skyrme form factor does not deviate appreciably from the covariant form factor, because even at smaller values of z the momentum transfers $|t|$ in fig. 4 are not large. One should also keep in mind that the reggeized pion has a variable spin different from zero, when t is different from the pole value. The coupling of virtual pions to the nucleon does not have to be identical to that imployed in one-pion-exchange potentials.

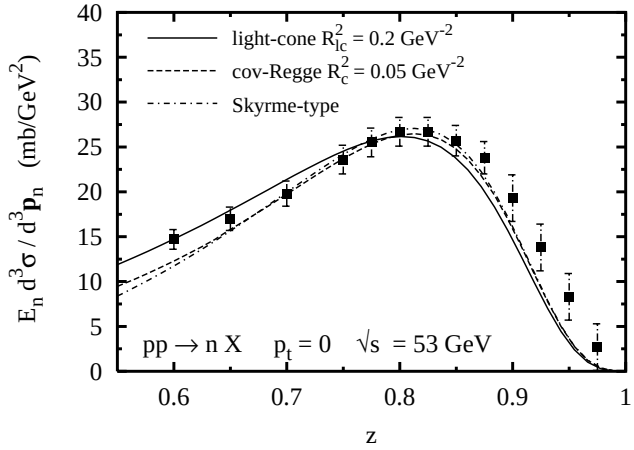

Fig. 4. Invariant differential cross sections for neutron production at $p_t = 0$ calculated according to eq. (20) for three different form factors. Data points are from ref. [24].

[5] In fig. 5 for $\sigma^{p\pi^+}_{\rm tot}$ we take directly the scattering data at small energies from the particle data group [26].

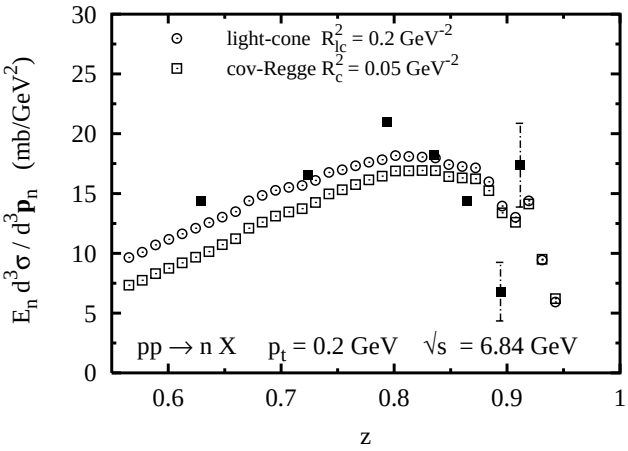

Fig. 5. Invariant differential cross sections for neutron production at $p_t = 0.2$ GeV calculated according to eq. (20) for two different form factors. Skyrme-type approach, not displayed, gives almost the same result as the covariant one. Points are low-energy $\sqrt{s} = 6.84$ GeV bubble chamber data, ref. [25].

The differences of the light-cone and covariant approaches are more pronounced for very large z and at $p_t \neq 0$. Here the light-cone form factor vanishes faster with z compared to the fall off in the reggeized covariant form factor. In fig. 5 we compare the light-cone and the covariant-Regge models with the invariant differential cross sections measured at $p_t = 0.2$ GeV [25]. The theory does not agree very well with these data. In fact these data are taken at $\sqrt{s} = 6.84$ GeV, where Feynman scaling is not expected to hold. One sees for the low-energy data that near $z = 0.9$ the $\pi^+ p$ resonances affect the cross section. There are also data at larger energies [28], but these do not cover simultaneously the large z and small p_t range.

The same calculation performed for the $pp \to nX$ reaction can be applied to $pn \to pX$, where the same $pn\pi$ vertex factor enters. The only changes to be done are $\sigma^{p\pi^-}$

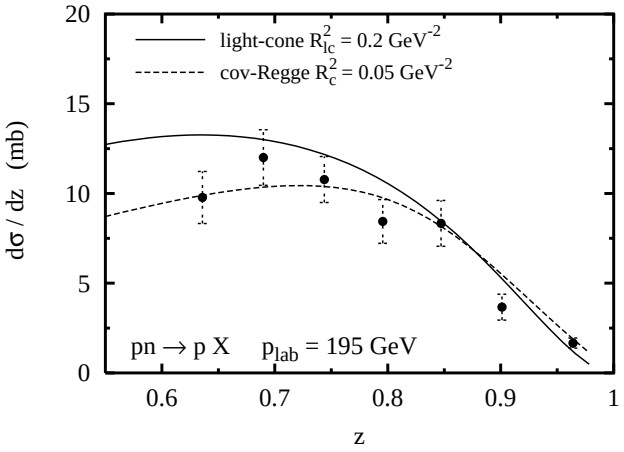

Fig. 6. Inclusive cross section for the $pn \to pX$ process at $p_{\rm lab} = 195$ GeV for $|t| < 1.4$ GeV^2, see text. Data points are from [29].

for $\sigma^{p\pi^+}$ and σ^{pp} for σ^{pn} in eq.(18). In fig.6 we show the p_t^2-integrated cross section for the $pn \to pX$ in light-cone and covariant-Regge pictures with the data from [29]. Again a reasonable agreement is found with the values of the radius parameters fitted on the leading neutron data at $p_t = 0$ (fig.4).

The effect of screening is shown clearly in fig. 7, where we plot the K-factor, i.e. the ratio of the differential cross section with and without absorptive corrections for the fitted values of the radii. The individual models differ slightly in the $z < 0.8$ region where there is a sizeable, $\geq 30\%$, screening. The light-cone form factor leads to a slightly smaller K-factor. For very large z values large transverse separations between the neutron and the pion dominate [17] (see fig. 3), thus the projectile proton misses the neutron for almost any finite impact parameter and the K-factor approaches unity.

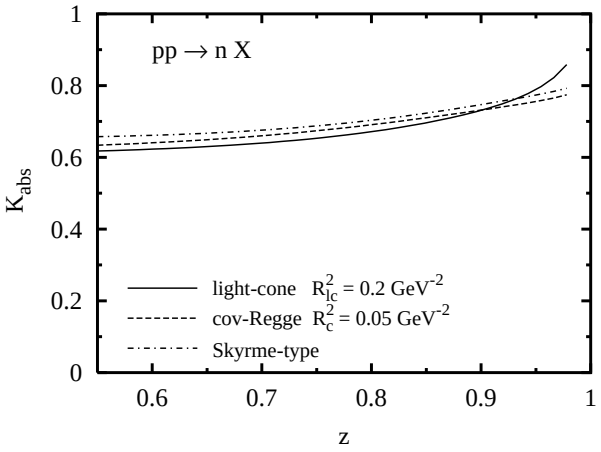

Fig. 7. Absorptive K-factors for neutron production in proton-proton collisions for three different form factors.

A comparison of the data with a calculation neglecting the screening mechanism would give larger radii. Such a fit can represent the data down to lower z values like $z = 0.65$. In general the amount of absorption can be reduced if one uses a larger cut-off radius in the pion form factor and additional exchanges [21]. An understanding of the trade-off between these two effects necessitates that they are considered together.

4 Cross sections for $\gamma^* p \to nX$ and $\gamma p \to nX$

In this section we consider the interaction of an initial virtual or real photon with a proton leading to neutron target fragments. Before entering the detailed calculation of the semi-inclusive reaction it is worthwhile to make some remarks on inclusive photon-nucleon interaction in context with our πNN form factor. Recently [20] an estimate of the antiquark distributions in the nucleon has been performed with the help of the Sullivan formula, cf. eq. (1). The calculation shows that for the Skyrme form factor used above the MCM prediction exhausts or only slightly exceeds the light sea quark distributions $\bar{u}$ and $\bar{d}$ in the proton at $Q^2 = 1.2\,\mathrm{GeV}^2$. This is a large improvement with respect to harder form factors often used before, which strongly overestimate this contribution. Thus the problems discussed e.g. in ref. [11] seem to be well taken care of. Two comments are in place: perhaps the F_2 calculations are not valid because of the interference between photon-nucleon and photon-pion inelastic interactions, where the target-like slow fragments of the struck sub-hadron and the residual hadron interact [17]. Since both are slow and strongly interacting there is no reason that this final state interaction is negligible. A second remark about the pion pole calculation is the possible contribution of diffractive excitation of the proton feeding the neutron channel. This problem has been investigated in [30]. Preliminary experiments [18] rather point to the fact that for $z < 0.8$ there is a sizable contribution of π_0-exchange to forward proton production [31].

A new approach [21] has been recently applied to describe in a consistent and unified framework proton fragmentation and the flavour asymmetry in the proton sea. This work [21] revises old form factor parametrizations and background contributions to one-pion-exchange in comparison with previous formulations in order to reproduce the new E866 data on the $\bar{u} - \bar{d}$ asymmetry.
We are aware that the models for the form factors we use here follow strongly the old approaches and therefore can not reproduce the new E866 data as well. As we limit our calculations to z-values bigger than 0.7, the issue of a quantitative description of the $\bar{u} - \bar{d}$ asymmetry is not so relevant [32].

In the semi-inclusive reaction we limit ourselves mainly to forward neutrons in photon induced reactions at small $x_{\rm Bj}$, as they are studied at HERA. In this kinematic region one cannot apply the usual factorization into a photon-quark cross section times a distribution function multiplied by a quark fragmentation function. That is why it is interesting by itself to study target fragmentation as

a nonperturbative process combining fragmentation and structure information. With good reason the new concept of fracture functions has been invented for this process. For small $x_{\rm Bj}$ we can consider the photon as a quark-antiquark state which materializes long before it reaches the proton [8] and interacts with the pion and neutron in the proton wave function. Schematically we write the inelastic cross section in a form similar to the proton induced one:

$$\sigma(\phi_0 \to \phi_\alpha) = \int d^2\mathbf{b} dw d^2\mathbf{r}\, |\Psi_{q\bar q}(w,\mathbf{r})|^2 \times \left|\langle \phi_\alpha[1 - S^{q\bar q\pi} S^{q\bar q n}]|\phi_0\rangle\right|^2 . \quad (22)$$

Here the $q\bar q$ pair wave function is represented by $\Psi_{q\bar q}(w,\mathbf{r})$ with w being the momentum fraction of the quark and $\mathbf{r}$ the transverse separation of the quarks. This wave function contains the summation over the electric charges of the different quarks and is electromagnetic in origin. The weak electromagnetic coupling determines the cross section of the photon with the pion.

Following the same procedure for the sum over all spatial configurations and over all excited (inelastic) states we get

$$\frac{d\sigma^{\gamma^* p\to nX}}{dz} = \int d^2\mathbf{b}_{rel}\rho_{n\pi}(z,\mathbf{b}_{rel}) \int d^2\mathbf{b} dw d^2\mathbf{r} |\Psi_{q\bar q}(w,\mathbf{r})|^2 \times 2Re\Gamma^{q\bar q\pi}(\mathbf{b}-\mathbf{s}_\pi,\mathbf{r})[1 - 2Re\Gamma^{q\bar q n}(\mathbf{b}-\mathbf{s}_n,\mathbf{r})] , \quad (23)$$

where we take into account the dependence on the $q\bar q$-size by an $\mathbf{r}$-dependent cross section:

$$\Gamma^{q\bar q a}(\mathbf{b},\mathbf{r}) = \frac{1}{4\pi}\sigma_{\rm tot}^{q\bar q a}(\mathbf{r}) \Lambda^2_{q\bar q a} \exp\Big[-\frac{\mathbf{b}^2\Lambda^2_{q\bar q a}}{2}\Big] . \quad (24)$$

By performing the $\mathbf{b}$-integration analytically we get

$$\frac{d\sigma^{\gamma^* p\to nX}}{dz} = \int d^2\mathbf{b}_{rel}\rho_{n\pi}(z,\mathbf{b}_{rel}) \int dw d^2\mathbf{r} |\Psi_{q\bar q}(w,\mathbf{r})|^2 \times \sigma_{\rm tot}^{q\bar q\pi}(\mathbf{r})\Big\{1 - \Lambda^2_{\rm eff}\frac{\sigma_{\rm tot}^{q\bar q n}(\mathbf{r})}{2\pi}\exp\Big[-\frac{\Lambda^2_{\rm eff}\mathbf{b}^2_{rel}}{2}\Big]\Big\} , \quad (25)$$

$$\text{with} \qquad \Lambda^2_{\rm eff} = \frac{\Lambda^2_{q\bar q\pi}\Lambda^2_{q\bar q n}}{\Lambda^2_{q\bar q\pi} + \Lambda^2_{q\bar q n}} . \quad (26)$$

In this form we see the role played by the photon wave function: It governs the integral but does not enter in the magnitude of the screening correction with the same weight as in the direct term. Screening is a strong interaction effect which is a function of the transverse size of the $q\bar q$ pair.

In the expression (25) we have a linear and a quadratic term in the dipole-hadron cross section $\sigma_{\rm tot}^{q\bar q h}(\mathbf{r})$ averaged on the photon wave function squared. The first is easily calculated giving the total photon-pion cross section,

$$\langle\sigma_{\rm tot}^{q\bar q\pi}\rangle \equiv \int dw d^2\mathbf{r}\, |\Psi_{q\bar q}(w,\mathbf{r})|^2 \sigma_{\rm tot}^{q\bar q\pi}(\mathbf{r}) = \sigma_{\rm tot}^{\gamma^*\pi} , \quad (27)$$

where we have introduced the notation of average to get simpler expressions in the following. The second term contains the correlated average of $q\bar q\pi$ and $q\bar q n$ cross sections. Equation (25) reads

$$\frac{d\sigma^{\gamma^* p\to nX}}{dz} = \int d^2\mathbf{b}_{rel}\rho_{n\pi}(z,\mathbf{b}_{rel})\, \sigma_{\rm tot}^{\gamma^*\pi^+} \times \Big\{1 - \Lambda^2_{\rm eff}\frac{\sigma_{\rm eff}}{2\pi}\exp\Big[-\frac{\Lambda^2_{\rm eff}\mathbf{b}^2_{rel}}{2}\Big]\Big\} , \quad (28)$$

where we have defined

$$\sigma_{\rm eff} = \frac{\langle\sigma_{\rm tot}^{q\bar q\pi}\sigma_{\rm tot}^{q\bar q n}\rangle}{\langle\sigma_{\rm tot}^{q\bar q\pi}\rangle} . \quad (29)$$

It is worthwhile to remind here that the total cross sections appearing in eqs. (28) and (29) depend on Q^2, the photon virtuality, and on the scaling variables x_π and x_n (respectively for a pion and a neutron target):

$$x_\pi = \frac{x_{\rm Bj}}{1-z} \qquad x_n = \frac{x_{\rm Bj}}{z} \qquad \text{with } x_{\rm Bj} = \frac{Q^2}{2q\cdot p} . \quad (30)$$

Aware of this we rewrite eq. (29) in the following way

$$\sigma_{\rm eff} = \frac{\langle\sigma_{\rm tot}^{q\bar q\pi}(x_\pi)\sigma_{\rm tot}^{q\bar q n}(x_n)\rangle}{\langle\sigma_{\rm tot}^{q\bar q\pi}(x_\pi)\rangle} = \frac{\langle\sigma_{\rm tot}^{q\bar q n}(x_\pi)\sigma_{\rm tot}^{q\bar q n}(x_n)\rangle}{\langle\sigma_{\rm tot}^{q\bar q n}(x_\pi)\rangle} , \quad (31)$$

where we use $\sigma_{\rm tot}^{q\bar q\pi} \propto \sigma_{\rm tot}^{q\bar q n}$, keeping the right x- and Q^2-dependences. The quantity in eq. (31) can be then be parametrized following Kopeliovich and Povh [33] as

$$\frac{\langle\sigma_{\rm tot}^{q\bar q n}(x_\pi)\sigma_{\rm tot}^{q\bar q n}(x_n)\rangle}{\langle\sigma_{\rm tot}^{q\bar q n}(x_\pi)\rangle} = N_0\frac{1}{F_2^p(x_\pi)}\left(\frac{1}{x_\pi}\right)^{\Delta_{\rm eff}}\left(\frac{1}{x_n}\right)^{\Delta_{\rm eff}} . \quad (32)$$

This parametrization is valid in the region of large Q^2 and small x values[6]. We choose the values $N_0 = 2$ GeV^{-2} and $\Delta_{\rm eff} = 0.15$ slightly different from those quoted in [33] as we are interested in a region of smaller x values. The low value for $\Delta_{\rm eff}$ comes from the fact that diffraction and therefore also shadowing are dominated by processes *softer* [8] than those dominating F_2^p for which we use the parametrization in the double leading log approximation [34] which covers a wide $x_{\rm Bj}$ and Q^2 range.

In the case of real photons at very high energies (HERA kinematics) we neglet the small effect in the difference between the photon-pion and photon-neutron cm-energies and get

$$\sigma_{\rm eff}|_{Q^2=0} = \frac{\langle(\sigma_{\rm tot}^{q\bar q n})^2\rangle}{\langle\sigma_{\rm tot}^{q\bar q n}\rangle} = \frac{16\pi}{\sigma_{\rm tot}^{\gamma p\to X}}\left.\frac{d\sigma^{\gamma p\to pX}}{dt}\right|_{t=0} = 16\pi\frac{b_D\sigma_D}{\sigma_{\rm tot}^{\gamma p\to X}} \approx 20\,{\rm mb} , \quad (33)$$

where we use $d\sigma^{\gamma p\to pX}/dt = b_D\sigma_D\exp(b_D t)$ with the experimental values for b_D and σ_D according to [35,36].

[6] Working at small $x_{\rm Bj}$ we can exchange all neutron labels against proton labels.

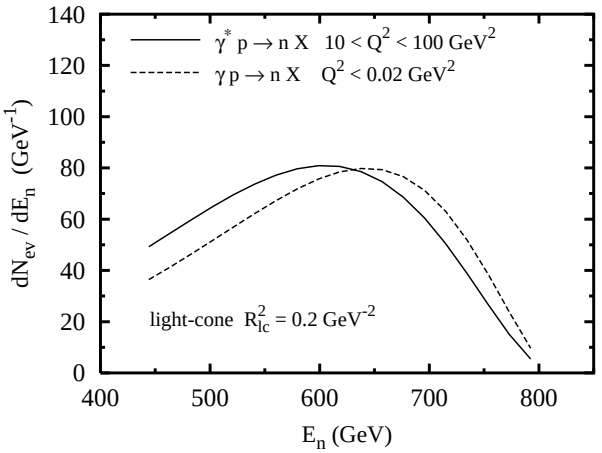

Fig. 8. Comparison of the energy distributions of neutrons for deep inelastic events and photoproduction imposing the kinematical cuts of ref. [1]. The distributions are normalized to the total number of DIS events.

Finally following the same idea of shadowing as a soft process which motivated the choice of $\Delta_{\rm eff}$ we employ slope parameters $\Lambda^2_{q\bar{q}n}$ and $\Lambda^2_{q\bar{q}\pi}$ which are calculated from total cross sections[7] $\sigma^{q\bar{q}n}_{\rm tot} = \sigma^{\rho n}_{\rm tot} \approx 30$ mb and $\sigma^{q\bar{q}\pi}_{\rm tot} \approx 20$ mb:

$$\Lambda^2_{q\bar{q}\pi} \approx \frac{4\pi}{\sigma^{q\bar{q}\pi}_{\rm tot}} \qquad \Lambda^2_{q\bar{q}n} \approx \frac{4\pi}{\sigma^{q\bar{q}n}_{\rm tot}}\,.$$

For the double differential $\gamma^* p$ cross section, we obtain with the help of eqs. (20) and (21),

$$\frac{d^2\sigma^{\gamma^* p\to nX}}{dz dp_t^2} = \frac{1}{N(z)}\frac{dN(z,p_t)}{dp_t^2}\,\frac{d\sigma^{\gamma^* p\to nX}}{dz}\,, \qquad (34)$$

which is then rescaled to yield the differential cross section for neutron production in electron-proton scattering (besides a small longitudinal contribution)

$$\frac{d^4\sigma^{ep\to e' nX}}{dx_{\rm Bj}dQ^2 dz dp_t^2} = \frac{\alpha_{\rm em}}{2\pi x_{\rm Bj}Q^2}\,(2-2y+2y^2)\,\frac{d^2\sigma^{\gamma^* p\to nX}}{dz dp_t^2}\,, \qquad (35)$$

with $y = \frac{Q^2}{x_{\rm Bj}s}$; s is the cm ep total energy squared. The phenomenological $\gamma^*\pi^+$ cross section entering eq.(28) is expressed in terms of the pion structure function

$$\sigma^{\gamma^*\pi^+}_{\rm tot}(x_\pi, Q^2) = \frac{4\pi^2\alpha_{\rm em}}{Q^2}F_2^{\pi^+}(x_\pi, Q^2)\,. \qquad (36)$$

In the following we use for demonstration purpose $F_2^{\pi^+}(x_{\rm Bj}, Q^2) = \frac{2}{3}F_2^p(x_{\rm Bj}, Q^2)$ valid at $x_{\rm Bj} \ll 0.1$. For real photons we refer to the fit performed in [27].

Averaging the colour dipole-neutron cross section together with the dipole-pion one, the decrease of the effective cross section $\sigma_{\rm eff}$ is less steep with increasing the virtuality of the photon than e.g. the free dipole-neutron cross section. Still screening is reduced for high Q^2. To show this we plot in fig. 8 the integrated neutron energy distributions in photoproduction with $Q^2 < 0.02$ GeV^2, 5 GeV $< E_e <$ 22 GeV, and in deep inelastic scattering with 10 GeV$^2 < Q^2 <$ 100 GeV^2, $0.04 < y < 0.95$, the ZEUS cuts ($\theta_{\rm scat} < 0.6$ mrad, $p_t < 0.5$ GeV and an integrated luminosity of 6.7 pb^{-1}). A shift of the DIS cross section maximum by 50 GeV to lower energies is clearly visible. This is due to screening, which reduces the cross section mainly at smaller E_n (neutron energy), such that the peak appears at higher energies in photoproduction. Our results indicate a clear signal for more transparency of the neutron when interacting with highly virtual photons. Small size color dipoles rescatter less on the target fragment neutron, even if for very large Q^2 screening still persists. The semi-inclusive reaction with Regge-exchange also allows to study the same phenomena as in the diffractive $\sigma^{\gamma^* p\to p+X}$ cross section.

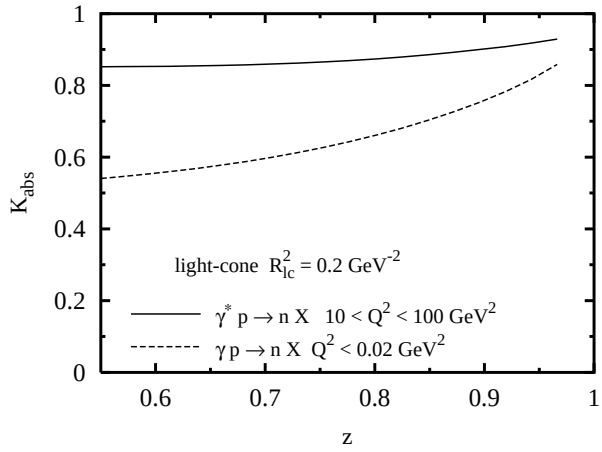

Fig. 9. Absorptive K-factor for neutron production in real and virtual photon-proton collisions.

The absorptive K-factors for $\gamma p \to nX$ and $ep \to e' nX$ are shown in fig. 9: it is visible that for DIS neutron production (high Q^2) screening becomes very weak , while for real photons we get, at large z, a somewhat reduced effect compared to proton-proton collisions (see fig. 7). For $z > 0.75$ and $Q^2 > 10$ GeV^2 the factorization of the cross section into a pion flux factor and a pion structure functions looks very acceptable.

In fig. 10 we show the p_t-integrated neutron cross section with the H1 cuts as function of z. The screening in $pp \to nX$ manifests itself as a bigger $ep \to e' nX$ cross section, since a higher pion flux is needed to explain the measured hadronic cross section. Notwithstanding the validity of the impuls approximation in high-Q^2 processes, factorization is broken in soft hadronic fragmentation reactions. The comparison of our result with the preliminary H1 data is very encouraging.

The fracture functions [6,7] introduced to describe target fragmentation allow a model independent evolution in

[7] From the neutron target to the pion target we scale total cross sections with the ratio of pion to proton size, i.e. with a factor 2/3.

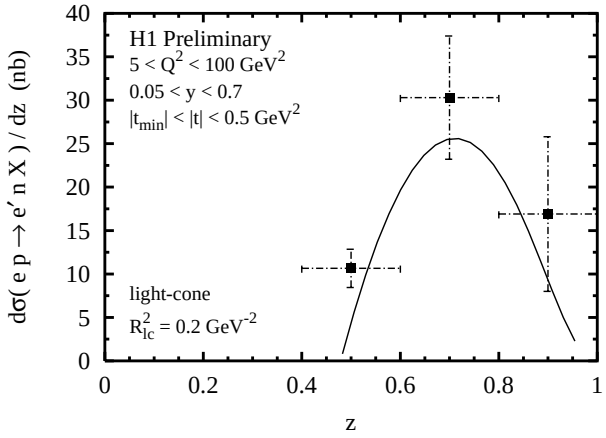

Fig. 10. Comparison of the differential cross section including screening corrections in light-cone approach with preliminary H1 data, ref. [2].

the framework of perturbative QCD, albeit the starting functions have to be known. In this approach the non-perturbative distributions are related to the p_t-integrated differential cross section for leading neutron production in ep scattering in the following way

$$\frac{d^3\sigma^{ep\to e'nX}}{dx_{\rm Bj}dQ^2dz} = \frac{2\pi\alpha_{\rm em}^2}{x_{\rm Bj}Q^4}(2-2y+2y^2)\, M_2(x_{\rm Bj},Q^2,z)\,, \quad (37)$$

where at leading order in α_s there is no contribution from the fragmentation of the struck quark in the target region. In the one-pion-exchange model without screening corrections one can interprete[8] $M_2(x_{\rm Bj},Q^2,z)$ as the product of the flux of neutrons integrated over p_t, times the pion structure function $F_2^\pi(x_\pi,Q^2)$.
The fracture function M_2 is defined in analogy with the structure function F_2,

$$M_2(x,Q^2,z) = x\sum_i e_i^2 M_{i,n/p}(x,Q^2,z)\,, \quad (38)$$

where $M_{i,n/p}(x,Q^2,z)$ represents the probability of finding a parton of flavour i with momentum fraction x and a neutron with momentum fraction z inside a proton.

In fig. 11 we give the fracture functions $M_2(x_{\rm Bj},Q^2,z)$ as functions of z, at fixed $x_{\rm Bj}$, for various Q^2 values.

The Q^2-evolution of the fracture functions we use is given at small virtualities by the higher twist effect of screening and at higher Q^2 by the evolution of the pion structure function. In fact for neutron fragmentation the Altarelli-Parisi evolution of the fracture function dominates the total Q^2-dependence as has been argued in ref. [37].

[8] Here one should consider this fracture function as an input distribution at a certain scale Q_0^2 and then apply the pQCD-evolution.

5 Discussion of fragmentation results and validity of the factorization hypothesis

Finally we compare the screening corrections for the three different cases of proton, real and DIS photon induced semi-inclusive fragmentation reactions (cf. figs. 7, 9). One sees that both proton induced and real photon induced cross sections have K-factors differing by about thirty percent from unity for $z < 0.8-0.9$. In this region factorization for these reactions does not hold. On the other hand for deep inelastic scattering at $Q^2 > 10$ GeV^2 the rescattering of the $q\bar{q}$ dipole in the photon by the neutron is weaker. The different sizes of the absorptive corrections in pp compared to $\gamma^* p$ interactions prevent a model independent extraction of F_2^π from the simple factorization hypothesis, in agreement with the conclusions reached in ref. [17]. We also show that the effect of rescattering for real photon-proton reactions is important and that one can disentangle the difference with highly virtual photons: the shift in the neutron energy distributions can be understood in terms of different absorption effects.

In addition an extraction of the pion structure function is affected by the uncertainty in the determination of the pion flux factor. Our fits to the proton induced fragmentation reaction give for the radius parameters $R_{lc}^2 = 0.2\,{\rm GeV}^{-2}$ and $R_c = 0.05\,{\rm GeV}^{-2}$. More accurate p_t neutron spectra in the case of deep inelastic scattering could reduce this uncertainty significantly. At the moment the p_t spectra in proton induced reactions have been measured for too low energies [25] or too high p_t in the relevant z range [28].

It may be added that other mechanisms in all three reactions start contributing for $z < 0.75$; ρ-exchange [3,4,21] has been added to the strong proton induced cross section presenting a non negligible contribution for $0.5 < z < 0.7$. In Monte Carlo simulations (LEPTO) the fragmentation cross section increases for $z < 0.5$. Further work is needed to understand this part of the cross section theoretically.

The semi-inclusive reactions in the large z-region show a case of transparency reminiscent of diffractive events. We think this finding of our paper merits a more accurate experimental examination. Exclusive (e.g. ρ-production) reactions are in seemingly good agreement with theoretical calculations based on the dipole picture, which is underlying color transparency. What is important to realize is that the final state interactions of virtual partons appear correlated with their initial state interaction.

Acknowledegments

We acknowledge many valuable discussions with J. Hüfner, B.Z. Kopeliovich, B. Povh, A. Schäfer, D. Jansen and T. Nunnemann. Special thanks go to N. N. Nikolaev for his kind help in revising the manuscript and pointing out the important reference [21].

U. D'Alesio was funded through the European TMR Contract No. FMRX-CT96-0008: Hadronic Physics with High Energy Electromagnetic Probes.

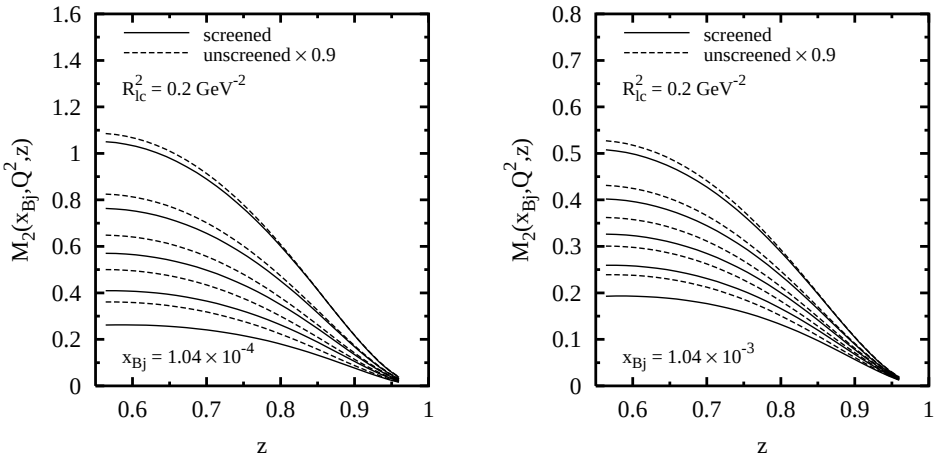

Fig. 11. Q^2-evolution of fracture functions $M_2(x_{\rm Bj}, Q^2, z)$ at fixed $x_{\rm Bj}$ as function of z. The Q^2 values are (from bottom to top) 2.5, 4.4, 7.5, 13.3, 28.6 GeV^2. Unscreened results are scaled by 0.9.

Appendix

Here we give the expression for the function entering the Skyrme-type form factor, eq. (6), [38]:

$$g(x) = 1 + \frac{\sum_{k=0}^{3} a_k T_k(\bar{x})}{1+mx}\,, \qquad x = \frac{|t|}{m_\pi^2}\,, \qquad \bar{x} = \frac{2x-a-b}{b-a} \tag{39}$$

where T_k is the k-th Tchebycheff polynomial of 1st kind, with $a = 0.003113 \quad b = 280.198488 \quad m = 10^{-8}$
$a_0 = 6.242336 \quad a_1 = 4.940353 \quad a_2 = 2.740654$
$a_3 = 0.9217577$.

References

1. ZEUS collab., Europhysics Conf. on High Energy Physics (641) Jerusalem 1997.
2. H1 collab., Europhysics Conf. on High Energy Physics (378) Jerusalem 1997.
3. H. Holtmann *et al.*, Phys. Lett. **B338** (1994) 363.
4. B.Z. Kopeliovich, B. Povh and I. Potashnikova, Z. Phys. **C73** (1996) 125.
5. G.F. Chew and F.E. Low, Phys. Rev. **113** (1959) 1640.
6. L. Trentadue and G. Veneziano, Phys. Lett. **B323** (1994) 201.
7. D. Graudenz, Nucl. Phys. **B432** (1994) 351.
8. N.N. Nikolaev and B.G. Zakharov, Z. Phys. **C49** (1991) 607.
9. V.R. Zoller, Z. Phys. **C53** (1992) 443.
10. H. Holtmann, A. Szczurek and J. Speth, Nucl. Phys. **A596** (1996) 631.
11. W. Koepf, L.L. Frankfurt and M. Strikman, Phys. Rev. **D53** (1996) 2586.
12. J.D. Sullivan, Phys. Rev. **D5** (1972) 1732.
13. M. Bishari, Phys. Lett. **B38** (1972) 510.
14. K.J.M. Moriarty, J.H. Tabor and A. Ungkichanukit, Phys. Rev. **D16** (1977) 130.
15. A.G. Azcárate, Phys. Rev. **D17** (1978) 3022.
16. B.G. Zakharov and V.N. Sergeev, Sov. J. Nucl. Phys. **28** (1978) 689; Sov. J. Nucl. Phys. **38** (1983) 801.
17. N.N. Nikolaev, J. Speth and B.G. Zakharov, hep-ph/9708290.
18. D. Jansen and T. Nunnemann, private communication.
19. G. Holzwarth and R. Machleidt, Phys. Rev. **C55** (1997) 1088.
20. R.J. Fries and A. Schäfer, hep-ph/9801358.
21. N.N. Nikolaev *et al.*, Phys. Rev. **D60** (1999) 014004.
22. A.Y. Abul-Magd and J. Hüfner, Nucl. Phys. **A308** (1978) 429.
23. A. Capella, J. Kaplan and J. Tran Thanh Van, Nucl. Phys. **B97** (1975) 493.
24. W. Flauger and F. Mönnig, Nucl. Phys. **B109** (1976) 347.
25. V. Blobel *et al.*, Nucl. Phys. **B135** (1978) 379.
26. Particle Data Group, Eur. Phys. J. **C3** (1998) 1.
27. A. Donnachie and P.V. Landshoff, Phys. Lett. **B296** (1992) 227.
28. J. Engler *et al.*, Nucl. Phys. **B84** (1975) 70.
29. Y. Eisenberg *et al.*, Nucl. Phys. **B135** (1978) 189.
30. H. Holtmann *et al.*, Z. Phys. **C69** (1996) 297.
31. A. Szczurek, N.N. Nikolaev and J. Speth, Phys. Lett. **B428** (1998) 383.
32. N.N. Nikolaev, private communication.
33. B.Z. Kopeliovich and B. Povh, hep-ph/9509362.
34. B.Z. Kopeliovich and B. Povh, Phys. Lett. **B367** (1996) 329.
35. M. Derrick *et al.* (ZEUS collab.), Z. Phys. **C75** (1997) 421; ZEUS collab., Eur. Phys. J. **C2** (1998) 237.
36. C. Adloff *et al.* (H1 collab.), Z. Phys. **C74** (1997) 221.
37. D. de Florian and R. Sassot, hep-ph/9703228.
38. R.J. Fries, private communication.